Neutron spectra from photonuclear reactions: performance testing of Monte-Carlo particle transport simulation codes

Valentin Blideanu, Clement Besnard Vauterin, David Horvath, Benoit Lefebvre, Francesc Salvat-Pujol, Roberto Versaci

Neutron spectra from photonuclear reactions: performance testing of Monte-Carlo particle transport simulation codes

C. Besnard-Vauterin[a], V. Blideanu[a], D. Horváth[b], B. Lefebvre[b], F. Salvat-Pujol[c], R. Versaci[b]

[a] *Université Paris-Saclay, CEA, List, Laboratoire National Henri Becquerel (LNE-LNHB) F-91129, Palaiseau, France*
[b] *The Extreme Light Infrastructure ERIC, ELI Beamlines Facility, Za Radnicí 835, Dolní Břežany 252 41, Czech Republic*
[c] *European Organization for Nuclear Research, 1 Esplanade des Particules, 1211 Geneva 23, Switzerland*

Abstract

The production of neutrons in photon-induced nuclear reactions in the giant-dipole-resonance energy domain remains a topic of high interest for various applications, including the activation and decommissioning of electron accelerator facilities, the detection of illicit materials for homeland security, and the evaluation of neutron dose received by patients during radiotherapy treatments. General-purpose Monte-Carlo (MC) simulation codes for particle transport are intensively used to account for photoneutron production in these applications. However, due to the current scarcity of measured photoneutron energy spectra in the literature, experimental validation of MC-simulated photoneutron energy distributions is not always feasible. Therefore, a critical benchmark among simulation results from various MC codes presently appears as the only option to systematically assess their capabilities in accurately simulating photoneutron production for nuclear reactions of interest. In this work, neutron energy spectra from several targets under irradiation by 20 MeV photons are simulated, employing various state-of-the-art MC codes (FLUKA, Geant4, MCNP6, and PHITS) in their default or generally employed settings. A detailed analysis of the simulated neutron spectra allows one to not only assess the performance of various MC codes in applications such as those mentioned above, but also to partially gauge the incurred systematic uncertainty, and to highlight the present need for more comprehensive evaluated nuclear data in this domain. Ultimately, this work suggests that more prudence is required when using MC codes for applications where photonuclear reactions play a dominant role and where not only the production rate but also the energy spectrum of the emitted neutrons matters.

Keywords: Photonuclear, Neutron production, Monte-Carlo, FLUKA, Geant4, MCNP6, PHITS

1. Introduction

Nuclear reactions induced by photons are of great interest, since they are the leading process in a variety of applications. For instance, in medical facilities employing linear electron accelera-

tors (LINACs) - about 4,000 in Europe and 13,000 worldwide - photonuclear reactions induced by Bremsstrahlung photons are not only responsible for a background dose delivered to the patient and affecting nearby accelerator components, but also directly affect the end-of-life decommissioning of such facilities, for which there is presently an increased demand for appropriate radioactive waste management. This has triggered a renewed interest in the characterization of the generated waste, by regulatory authorities and waste-management operators alike, in order to identify suitable waste management options [1]. Likewise, active photon interrogation in photoneutron spectrometry presently constitutes a very promising option for the detection of illicit materials through photonuclear reactions on light elements such as carbon, oxygen and nitrogen, usually present in explosive compounds, narcotics, and chemical weapons [2, 3, 4, 5].

Considering the widespread reliance on general-purpose Monte-Carlo (MC) simulation codes for particle transport to assess photoneutron production in the aforementioned applications, a critical assessment of their capabilities and performances is necessary. In view of the current scarcity of experimental neutron energy spectra from nuclei under photon irradiation [6, 7], code benchmarking and intercomparison appears as the next best avenue, not only to assess the performance of various MC codes, but also to estimate the model-dependent systematic uncertainty incurred when assessing the importance of photoneutron production in various neutron energy domains relying on well-established MC simulation codes.

In this work, the energy spectrum of neutrons emitted from thin slabs of a series of materials ranging from beryllium to lead in natural composition under irradiation by 20 MeV photons is estimated, employing various state-of-the-art codes for the MC simulation of radiation transport (FLUKA, Geant4, MCNP6, and PHITS), using the methodology detailed in Sec. 2. The simulated neutron energy spectra are presented in Sec. 3, where relevant differences are highlighted and analyzed, showcasing the considerable spread among various simulation calculations in this domain. The integrated cross section for photoneutron production yielded by the selected MC codes is discussed and compared against experimental data in Sec. 4. Finally, a condensed summary and conclusions from the present simulation benchmark, as well as a remark highlighting the need for further experimental data in this domain, are presented in Sec. 5.

2. Methodology

To showcase differences in neutron production from nuclei under photon irradiation among various MC codes, a common simulation setup has been adopted, consisting of a thin target disk (1 mm thickness and 1 cm diameter) made of the various target materials discussed below, immersed in vacuum. The thickness of 1 mm was chosen as to significantly reduce the probability of secondary hadron re-interaction, while photonuclear interactions were explicitly biased in order to enhance the

efficiency of the present thin-target simulation when using MC codes offering this capability (see Sec. 2.2). The target is uniformly irradiated with a monoenergetic 20 MeV parallel photon beam, with a diameter of 1 cm, precisely extending over circular base of the cylindrical sample and impinging normally along its symmetry axis. The selected photon energy does not only represent typical Giant Dipole Resonance energies, but is also of eminent practical relevance for the aforementioned applications. For instance, medical LINACs are easily able to produce such energetic photon beams. Moreover, photons in the energy range from 15 to 20 MeV are optimal candidates for illicit material detection based on active photon interrogation [5].

2.1. Target materials

A variety of target materials has been considered in this work, in order to cover a wide range of nuclei masses relevant for the aforementioned applications. Beryllium, aluminum, copper, antimony, tungsten, and lead have been considered, since these materials are present in significant quantities in the components of medical LINACs. Lighter nuclei such as carbon and nitrogen have also been included, in view of their biological relevance. Nitrogen is particularly interesting, since its photoneutron spectrum can be used as a marker for illicit materials including explosives, drugs, and chemical agents [8, 5].

2.2. Methods

Four well-established and widely used general-purpose codes for the MC simulation of particle transport have been used in this work: FLUKA, Geant4, MCNP6, and PHITS. In the following sections, the main features of each code are outlined, highlighting the most relevant aspects for photoneutron production. Statistical error bars in the various simulated neutron spectra displayed below are of the order of 1% and have been omitted for clarity.

2.2.1. FLUKA

FLUKA [9, 10, 11] is a general-purpose MC simulation code for particle transport, developed by the FLUKA.CERN Collaboration. It models the transport and interaction of hadrons, ions, leptons, and photons over wide energy ranges in complex geometries.

In the energy range considered in this work (20 MeV excitation energy), FLUKA treats photonuclear interactions [12] via a pre-equilibrium stage (including a nucleon coalescence model) followed by an evaporation stage (with a Fermi break-up model for targets with mass number $A < 18$ [13]), both including spin- and parity-conservation considerations, with a final gamma de-excitation cascade [14, 15, 16]. The photonuclear interaction rate in FLUKA is driven by a photonuclear absorption cross-section library derived from evaluated nuclear data for almost 200 target nuclides, complemented by effective parametrized cross-sections for the rest of nuclides [17].

FLUKA v4-3.0 has been used in this work, with photonuclear interactions activated explicitly. The nuclear inelastic scattering length of primary photons has been biased by a reduction factor of 100, properly taken into account in particle statistical weights.

2.2.2. Geant4

Geant4 [18, 19, 20] is a multi-purpose particle propagation MC code, distributed as a toolkit of C++ libraries, developed and maintained by the Geant4 collaboration. For the results presented here, a custom program including relevant libraries of Geant4 version 11.1.1 was written in C++ to handle the event generation, the definition of the simulation geometry and media, and scoring.

Geant4 users are responsible for choosing the simulation physics settings (the so-called physics list) that are best suited for the requirements of their application. Thus, two particular settings have been considered in this work. On the one hand, the `FTFP_BERT` physics list was considered, since it is recommended as a generally applicable default in the official Geant4 guide for physics lists [21]. Within this physics list, photonuclear interactions below 6 GeV are simulated by the Bertini model. On the other hand, the `Shielding` physics list, recommended for simulation of deep shielding, was used, with the `LEND` option, because the latter is prescribed for incident photons below 20 MeV.

The physics settings of the simulation were modified by biasing photon interactions in the target using a `G4GenericBiasingPhysics` object and the `G4VBiasingOperator` class. The biased processes are configured such that the interaction lengths for photon processes are reduced by a factor of 10 and particles weights adjusted accordingly. While the chosen factor here (10) is different than that used for FLUKA simulations (100), the net effect is a mere difference in the simulation efficiency. Since perfect vacuum is not permitted within Geant4, the medium surrounding the target is modelled as a material with the same composition as air but with a density of 10^{-25} g/cm^3.

2.2.3. MCNP6

The MCNP6 code [22] is a general purpose, continuous-energy, generalized-geometry, time-dependent code designed to track 37 particle types over a broad energy range. Version 6.2 was used in the present study.

Its capability to simulate photonuclear reactions was introduced in 2000 through evaluated cross-section libraries [23]. The one used here is known as the LA150 library [24]. It comprises a complete photonuclear evaluation in the ENDF-6 format [25] for several elements. It was published under the "24u" library ID as the LA150u ACE library (see ref. [26]) and was used for MCNP6 simulations as the default library for photonuclear physics.

As for the inputs, the main concern is that MC sampling of the evaluated cross-section libraries is inherently limited by their availability. In the present study, materials cards were specified using

isotopic nuclei identifiers. For each of them, considered neutron and photonuclear transport data are taken from the only available LA150 library. The lack of a needed table is normally handled by using physics models but this was not the case for the materials considered in this study. No biasing techniques were used for the calculations with MCNP6.

2.2.4. PHITS

PHITS [27, 28, 29, 30] is a general-purpose MC particle transport simulation code developed in collaboration among JAEA, RIST, KEK and several other institutes. It can deal with the transport of all common particles over wide energy ranges, using several nuclear reaction models and cross-section libraries.

Starting from version 2.64, PHITS uses the evaluated cross-section libraries from JENDL/PD-2016, with a modification of the evaporation model for the giant resonance of some light elements considering the branching ratios calculated using the isospin selection rule [31]. Although since version 3.27 of PHITS it is possible to read external photonuclear cross-section libraries in the ACE format – as it is done with MCNP6 – to get model-dependent results, all of the PHITS results presented in this work are achieved with the default photonuclear library "51u".

In the simulations, the photon transport and interactions are handled by the EGS5 algorithm. Photonuclear interactions are activated, except for the process of nuclear resonance fluorescence. No biasing was applied to photonuclear interactions.

3. Results

In the following subsections, neutron spectra obtained with FLUKA, Geant4, MCNP6, and PHITS for the simulation setups described in Sec. 2 are presented, both in the linear and logarithmic abscissa scales, in order to better resolve the higher and lower ends of the photoneutron energy spectrum, respectively. The aim of the subsequent discussion of the simulated neutron spectra is not to analyze every spectral feature, but to highlight the most relevant differences among results obtained with the various MC codes.

The presence of discrete nuclear energy levels, usually well separated for light nuclei, gives the energy spectrum of emitted photoneutrons the particularity of exhibiting peaks at well-defined energies. For the channel (γ, n), with no ejectile involved other than the neutron and the residual nucleus, the emitted neutron energy may be estimated as follows [3]:

$$E_n = \frac{E_\gamma - Q - E_{\text{state}}}{1 + A_{\text{residual}}^{-1}} \,, \tag{1}$$

where E_γ is the incident photon energy, Q is the reaction Q value, E_{state} is the energy of the excited state of the residual nucleus, and A_{residual} is the mass number of the residual nucleus.

Note, however, that all neutron spectra presented below are inclusive spectra, i.e. they contain not only the explicit contribution of (γ, n), but also, where applicable, that of (γ, Xn), involving the subsequent emission of multiple neutrons, and even the contribution of possibly open channels involving the emission of charged particles [32], e.g. (γ, pn).

3.1. Beryllium

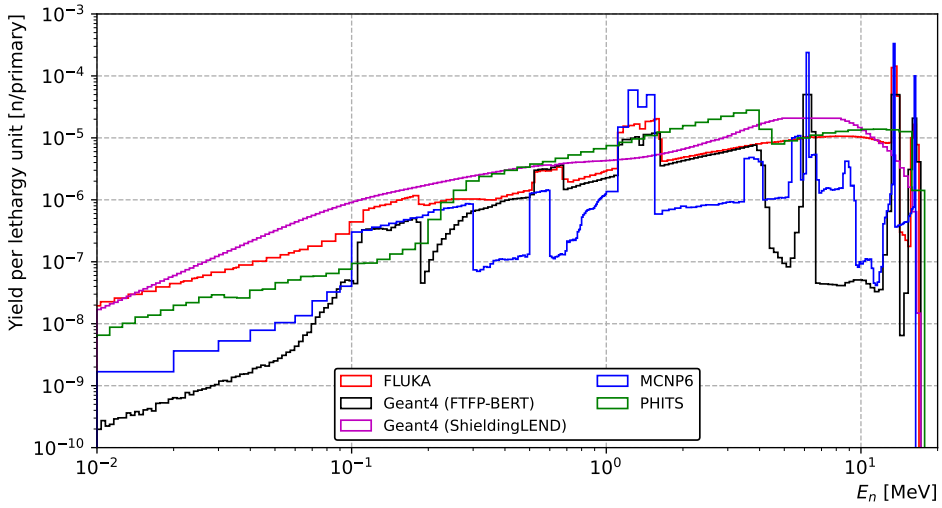

(a)

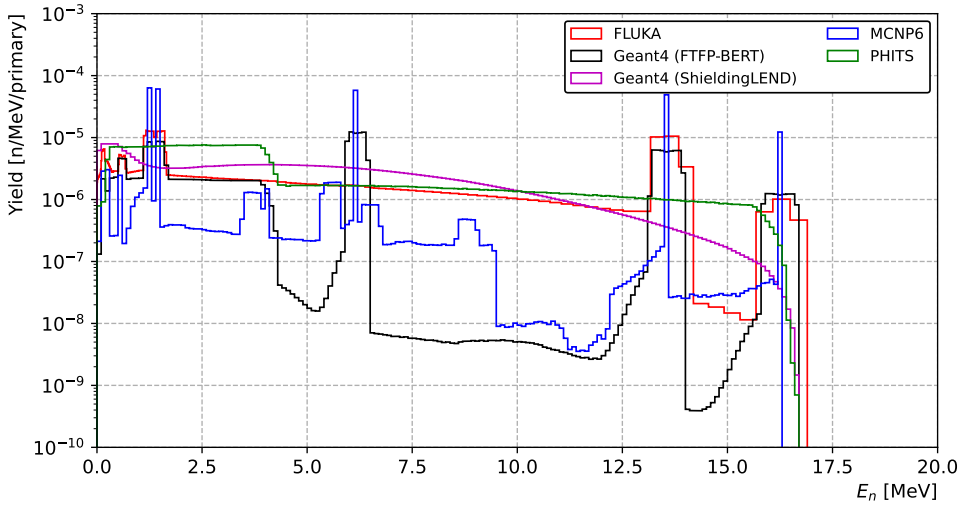

(b)

Figure 1: Simulated energy spectra of neutrons escaping the beryllium target in (a) logarithmic and (b) linear energy scale.

Beryllium is the lightest target nucleus considered in this study, and can be found in accelerator environments, for instance in vacuum windows and as a target. A density of 1.84 g/cm^3 was taken in the simulations reported here. ^{9}Be has its Q value for the ^{9}Be$(\gamma, n)^8$Be reaction at -1.6654 MeV, which is the highest among all the considered nuclides. As for the other samples, Q values are taken from the nuclear datasheets.

Figure 1 displays the energy spectrum of neutrons emitted from ^{9}Be under irradiation by 20 MeV photons, obtained with FLUKA, Geant4 (both with `FTFP_BERT` and `ShieldingLEND`), MCNP6, and

PHITS, both in logarithmic (upper plot) and linear (lower plot) scale. Statistical uncertainty bars have been omitted in all spectra for clarity. Several preeminent peaks are observed, as a signature of the (γ, n) process leaving the residual ^{8}Be in various excited levels before de-exciting, typically through the subsequent break-up into two α particles for the lower-lying excited levels.

Table 1 displays the excitation energy of the first few excited levels of the residual ^{8}Be, obtained from ref. [33], as well as the neutron laboratory kinetic energy for the (γ, n) channel. These peaks are overlaid on top of a broader background due to reaction paths involving the subsequent emission of further particles besides the neutron, *e.g.* ^{9}Be(γ,n$\alpha\alpha$), ^{9}Be(γ,pn)^{7}Li$_{\mathrm{gs}}$, and ^{9}Be(γ,pn)^{7}Li$_{1^{\mathrm{st}}}$, the latter accompanied by the emission of a 477 keV photon (Doppler broadened).

As illustrated in Fig. 1, all (γ, n) photoneutron peaks reported in Tab. 1 are present in the spectra from Geant4 (with `FTFP_BERT`), FLUKA, and MCNP6, with the exception of the 6.20 MeV photoneutron peak (corresponding to a reaction path through the second excited level of ^{8}Be), which is absent in the FLUKA spectrum. The Geant4 `ShieldingLEND` spectrum is lacking the peak structure; it provides instead an average description of the neutron yield, with a substantially higher intensity than that of the `FTFP_BERT` yield. FLUKA and Geant4 (with `FTFP_BERT`) exhibit wide peaks (around 1 MeV wide), suggesting that photoneutrons are emitted isotropically in the center of mass frame and are Doppler broadened when boosting to the lab frame. MCNP6 instead exhibits discrete peaks, resolved here within the 200 keV histogram bin width. PHITS exhibits a completely different behavior. By default, it employs the photonuclear reaction cross sections contained in the JENDL/PD-2004 database, but the energy of the secondary neutrons produced by photonuclear reactions is determined by a model (involving an evaporation stage), which does not capture the discrete sharp peaks due to the nuclear level structure.

Energy level of ^{8}Be [MeV ± keV]	Photoneutron energy [MeV]
g.s. (ground state)	16.48
3.03 ± 10	13.60
11.35 ± 150	6.21
16.626 ± 3	1.52
16.922 ± 3	1.26
17.640 ± 1	0.66
18.150 ± 4	0.16

Table 1: Energy levels of ^{8}Be obtained from ref. [33] and corresponding photoneutron energies for the various channels ^{9}Be(γ,n)^{8}Be$_{\mathrm{gs,1^{st},2nd,...}}$.

3.2. Carbon

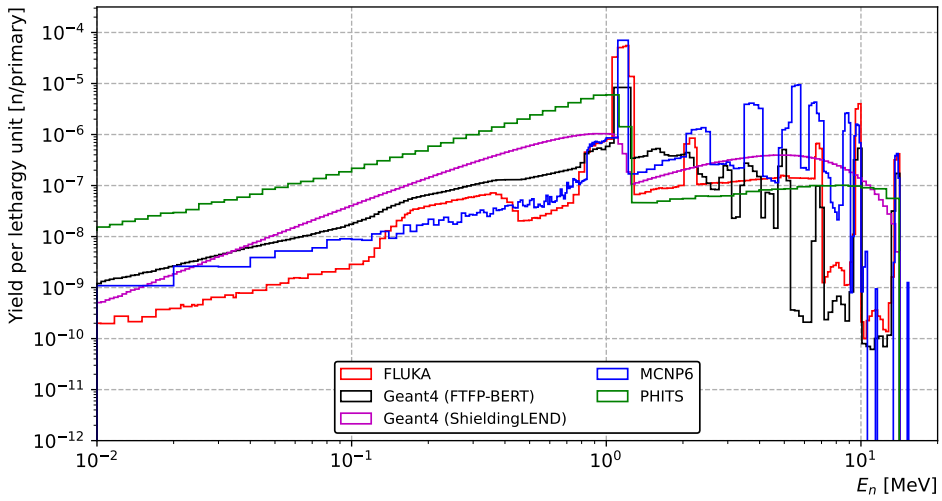

(a)

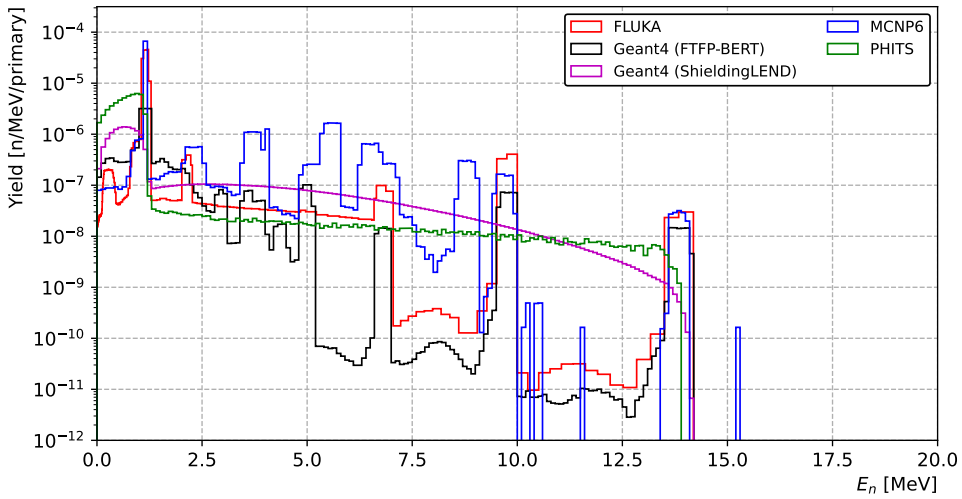

(b)

Figure 2: Simulated energy spectra of neutrons escaping the carbon target in (a) logarithmic and (b) linear energy scale.

In the present study, carbon was also considered as target material, with natural isotopic composition (98.9% of ^{12}C and 1.1% of ^{13}C) and a density of 2 g/cm^3. The Q values for the $^{12}\mathrm{C}(\gamma, n)^{11}\mathrm{C}$ and the $^{13}\mathrm{C}(\gamma, n)^{12}\mathrm{C}$ reactions are respectively -18.7217 MeV and -4.94634 MeV. Figure 2 displays the emitted photoneutron spectrum from $^{\mathrm{nat}}$C under irradiation by 20 MeV photons, in logarithmic (upper plot) and linear (lower plot) energy scale, for the various MC codes considered in this study. Once again, a series of conspicuous peaks is encountered. For the channel $^{12}\mathrm{C}(\gamma, n)^{11}\mathrm{C_{gs}}$, a photoneutron peak is expected around 1.24 MeV and is duly reproduced by all codes considered here, with the exception of Geant4 (with `ShieldingLEND`) and PHITS. It is interesting to consider that

the first excited level of the residual ^{11}C is at 2 MeV ± 0.4 keV [34]. The channel $^{12}\mathrm{C}(\gamma,n)^{11}\mathrm{C}_{1\mathrm{st}}$ therefore requires a photon threshold energy of 20.74 MeV, which exceeds the primary photon energy in this study. Thus, no signature from excited states of the residual ^{11}C is found in the simulated photoneutron spectra.

Further peaks in the neutron energy spectrum are a signature of various $^{13}\mathrm{C}(\gamma,n)^{12}\mathrm{C}$ channels, leaving the residual ^{12}C in the ground state or in the first few low-lying excited states, whose excitation energies are reported in Tab. 2, along with the corresponding estimated neutron peak energies. FLUKA, Geant4 (with `FTFP_BERT`), and MCNP6 all capture the peak corresponding to the ground state as well as the first and second excited states of the residual nucleus, although peak intensities may vary by up to an order of magnitude among codes. These peak intensities are roughly a factor of 100 lower than those for $^{12}\mathrm{C}(\gamma,n)^{11}\mathrm{C}$, reflecting the much lower abundance of ^{13}C in $^{\mathrm{nat}}$C (the photonuclear reaction cross section for ^{13}C is a factor ~ 2.4 higher than for ^{12}C, so it plays a minor role in front of the isotopic abundance). The photoneutron peaks at 4.99 MeV and 3.88 MeV are only shared by MCNP6 and Geant4 (with `FTFP_BERT`). The photoneutron peaks at 4.78 MeV and 2.97 MeV are only exhibited by Geant4 (with `FTFP_BERT`). The Geant4 `ShieldingLEND` spectrum is lacking the peak structure, but still provides an overall average description of the neutron yield as a bimodal distribution, yielding however a higher yield than that of `FTFP_BERT`. Additionally, MCNP6 yields two other peaks at around 6 MeV and 8.5 MeV that do not appear to arise from the $^{13}\mathrm{C}(\gamma,n)^{12}\mathrm{C}$ reaction. Incidentally, the broad background feature at low energies extending up to about 7 MeV has contributions from the channel $^{13}\mathrm{C}(\gamma,n3\alpha)$. Instead, the continuum features extending from $\sim$ 10 MeV down to $\sim$7 MeV and from $\sim$ 14 MeV down to $\sim$ 10 MeV are exclusively due to neutrons which, in spite of the thin sample, undergo a nuclear elastic interaction along their transport out of the target disk. While this process is certainly also likely in the beryllium target discussed in the preceding section, its effect is visible in a spectral energy range where (unlike for the carbon target) other channels already contribute and dominate. The peak visible in the MCNP6 spectrum beyond 14.06 MeV is kinematically not expected to arise directly from the $^{13}\mathrm{C}(\gamma,n)^{12}\mathrm{C}$ or $^{12}\mathrm{C}(\gamma,n)^{11}\mathrm{C}$ reactions.

Energy level of ^{12}C [MeV ± keV]	Photoneutron energy [MeV]
g.s.	14.06
4.43982 ± 0.21	9.79
7.65407 ± 0.19	6.83
9.641 ± 5	4.99
9.870 ± 60	4.78
10.847 ± 4	3.88
11.836 ± 4	2.97
12.710 ± 6	2.16
13.316 ± 20	1.60
14.079 ± 5	0.90

Table 2: Energy levels of ^{12}C from ref. [35] and corresponding photoneutron energies for the various channels $^{13}\mathrm{C}(\gamma,\mathrm{n})^{12}\mathrm{C}_{\mathrm{gs,1^{st},2nd...}}$.

3.3. Nitrogen

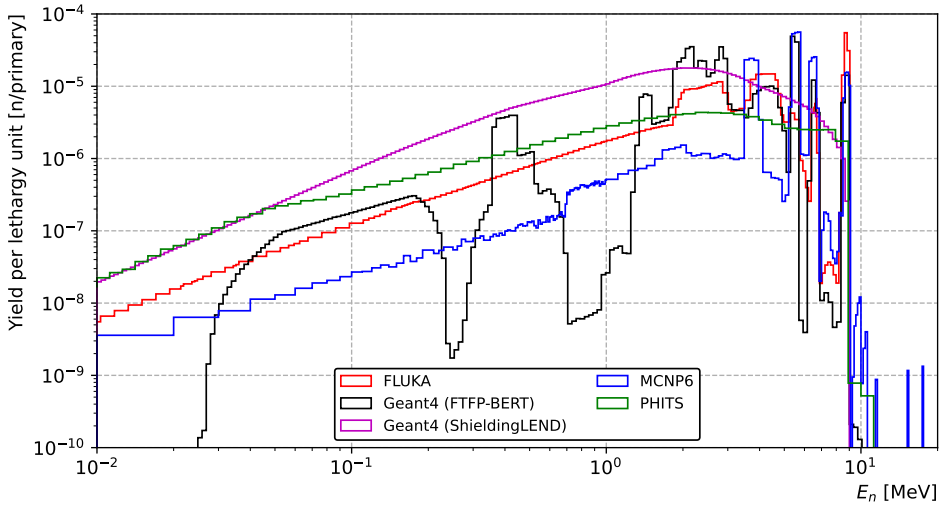

(a)

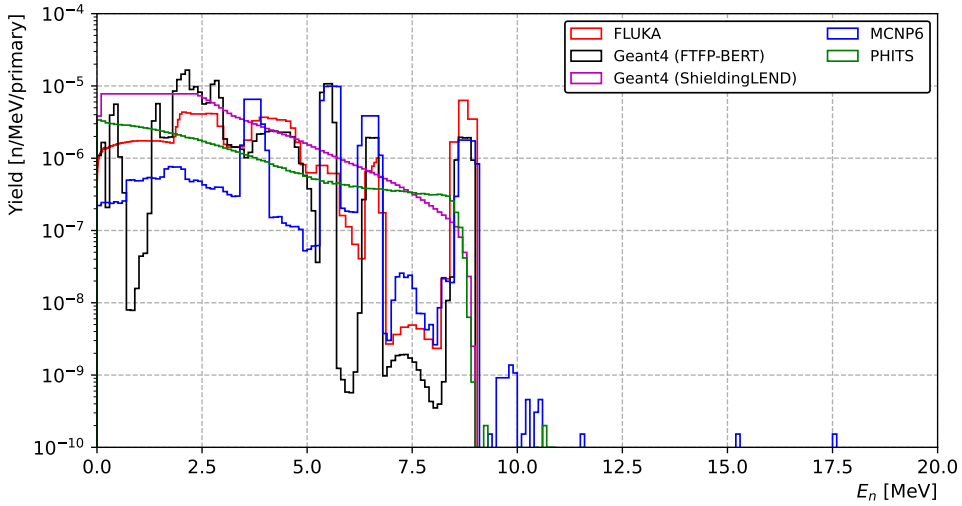

(b)

Figure 3: Simulated energy spectra of neutrons escaping the nitrogen target (density of 1 g/cm^3) in (a) logarithmic and (b) linear energy scale.

Nitrogen is also considered in this study, because its photoneutron spectrum is used as a marker for the detection of conventional explosives, chemical weapons, narcotics, drugs, especially in view of the recent emergence of compounds related to opioids [2]. It was taken in its natural composition (99.6% of ^{14}N and 0.4% of ^{15}N) in the simulations reported here, with an artificially high density of 1 g/cm^3 in order to enhance simulation convergence for MC codes with no built-in option to bias nuclear inelastic interactions. Tables 3 and 4 display the first few energy levels of the residual ^{13}N and ^{14}N [36], as well as the corresponding expected photoneutron energies, both for the ^{14}N$(\gamma, n)^{13}$N

and the $^{15}N(\gamma, n)^{14}N$ channels. Q values for those reactions are respectively : -10.554 MeV and -10.8333 MeV. It is interesting to note that neutrons emitted from these channels, leaving the residual nucleus in the ground state and in the 1^{st} excited state, have very similar energies, regardless of whether they are emitted via the former or the latter channel. Thus, instead of four discrete peaks, two groups of two largely overlapping peaks are expected.

Figure 3 shows that Geant4 (with `FTFP_BERT`), MCNP6, and FLUKA photoneutron spectra share the neutron peaks leaving the residual nucleus in the ground state and the first three excited states, from what is most likely ^{13}N as per its dominant abundance in natural composition. The Geant4 `ShieldingLEND` spectrum provides an average overall description, exhibiting a somewhat higher intensity with respect to the rest of spectra. The Geant4 `FTFP_BERT` features below 1 MeV are not displayed by the rest of yields. It is worth noting that MCNP6 is presenting a photoneutron peak at around 3.75 MeV, while Geant4 (with `FTFP_BERT`) and FLUKA are showing features around 4.5 MeV and 2.5 MeV. The MCNP6 peaks beyond 9.5 MeV appear to be beyond what one would kinematically expect from the primary (γ,n) reaction. The broad continuum below 2 MeV has contributions from the channels $^{15}N(\gamma,pn)^{13}C$ and $^{14}N(\gamma,pn)^{12}C$, the latter being left either on the ground state or in the first excited state, with the subsequent emission of a (Doppler-broadened) 4.4 MeV photon.

Energy level of ^{13}N [MeV ± keV]	Photoneutron energy [MeV]
g.s.	8.92
2.3649 ± 0.6	6.58
3.502 ± 2	5.52
3.547 ± 4	5.48
6.364 ± 9	2.87
6.886 ± 8	2.38
7.155 ± 5	2.13

Table 3: Energy levels of ^{13}N and corresponding photoneutron energies for the various channels $^{14}N(\gamma,n)^{13}N_{gs,1^{st},2nd}$.

Energy level of ^{14}N [MeV ± keV]	Photoneutron energy [MeV]
g.s.	8.69
2.312798 ± 0.011	6.35
3.94810 ± 0.20	5.29
4.9151 ± 1.4	5.25

Table 4: Energy levels of ^{14}N and corresponding photoneutron energies for the various channels ^{15}N $(\gamma,n)^{14}N_{gs,1^{st},2^{nd},...}$.

3.4. Aluminum

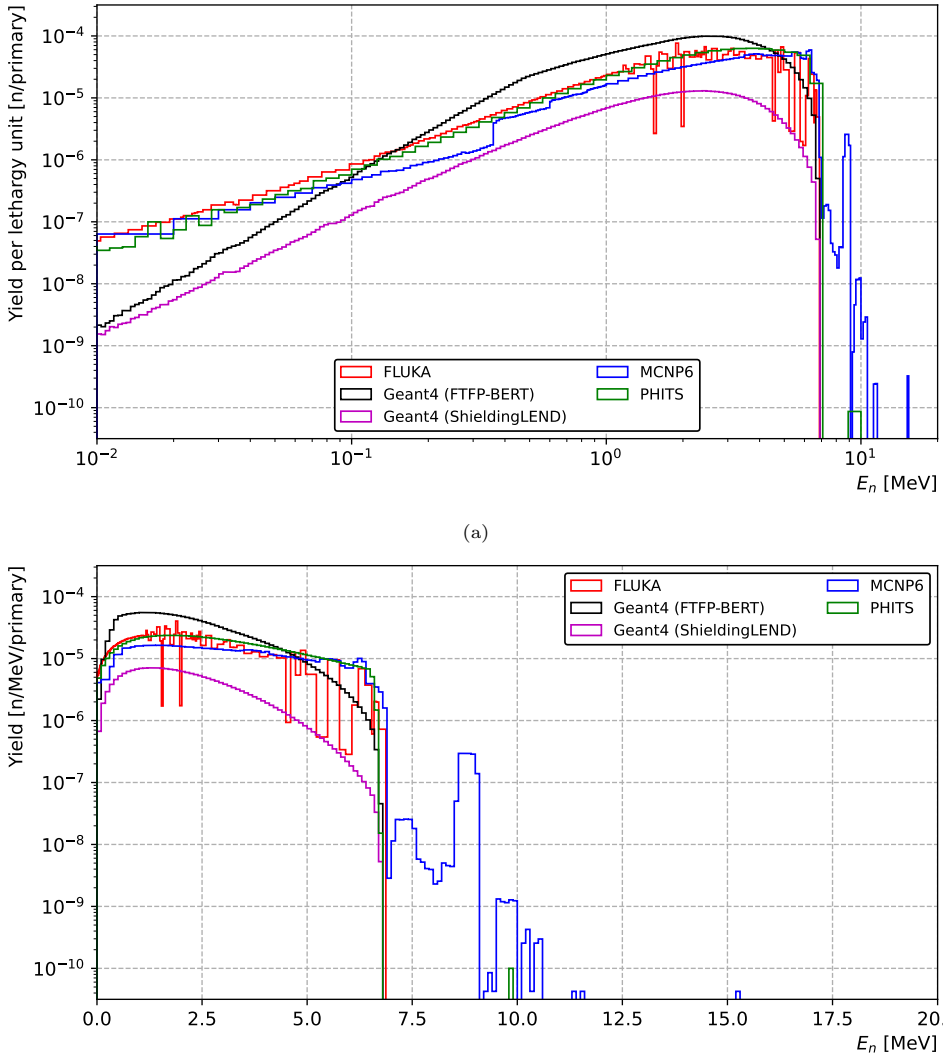

Figure 4: Simulated energy spectra of neutrons escaping the aluminum target in (a) logarithmic and (b) linear energy scale.

Aluminium has also been considered in this study, in view of its widespread use *e.g.* in medical accelerators, benefiting from its low density. Its natural composition (isotopically pure ^{27}Al) has been adopted, with a standard density of 2.7 g/cm^3. The Q value for the $^{27}\mathrm{Al}(\gamma, n)^{26}\mathrm{Al}$ reaction is -13.057 MeV.

Figure 4 displays the emitted neutron energy spectrum simulated with the various codes, in the logarithmic (upper plot) and linear (lower plot) energy scale as in the previous sections. A very reasonable agreement is obtained among the FLUKA, MCNP, and PHITS simulation results.

Traces of discrete peaks are now more difficult to resolve (exhibited only by the FLUKA spectrum), in view of the fact that energy levels of the residual ^{26}Al are considerably more densely packed than for the lighter elements considered in the foregoing sections. This is precisely the reason why for Al and the heavier targets considered below PHITS spectra are in overall very good agreement with the rest of codes. The Geant4 spectra, while extending to the correct kinematical limit and exhibiting a continuum as well, display a somewhat different spectral shape, slightly stressing neutron energies from 0.5 to 4 MeV, at the expense of energies below 0.5 MeV. The Geant4 `FTFP_BERT` neutron yield is higher than that of Geant4 `ShieldingLEND`. As was the case for the lighter materials, MCNP6 spectra exhibit features beyond what one would kinematically expect for the (γ, n) channel.

Tables 5 displays the first few energy levels of the residual ^{26}Al [37], as well as the corresponding expected photoneutron energies.

Energy level of ^{26}Al [MeV ± keV]	Photoneutron energy [MeV]
g.s.	6.76
0.228 ± 13	6.47
0.416 ± 3	6.29
1.057 ± 12	5.67
1.759 ± 8	5.00
1.850 ± 3	4.91

Table 5: Energy levels of ^{26}Al and corresponding photoneutron energies for the various channels $^{27}\mathrm{Al}(\gamma,\mathrm{n})^{26}\mathrm{Al}_{\mathrm{gs},1^{\mathrm{st}},2^{\mathrm{nd}},\ldots}$.

3.5. Copper

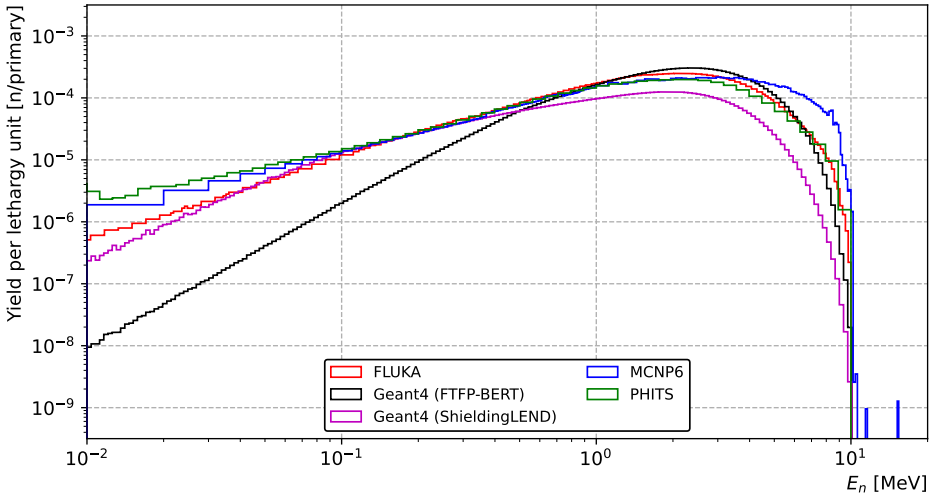

(a)

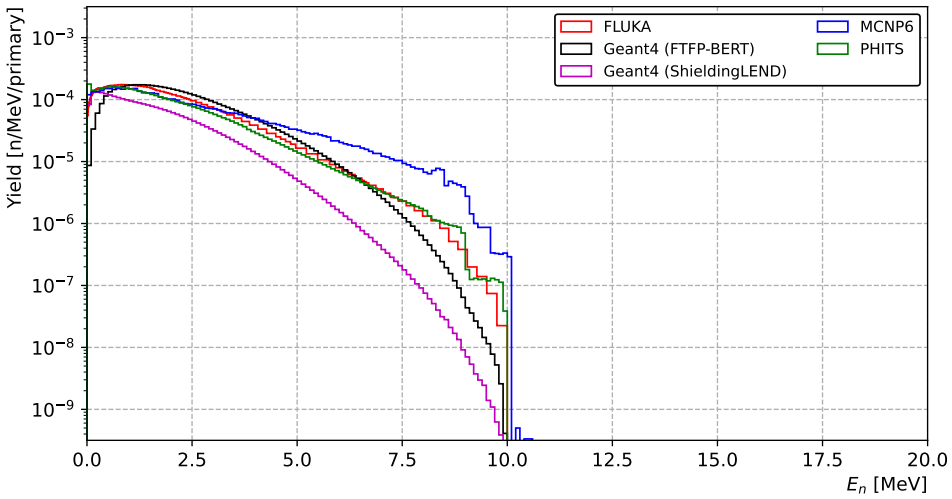

(b)

Figure 5: Simulated energy spectra of neutrons escaping the copper target in (a) logarithmic and (b) linear energy scale.

Natural copper is another heavily used building material when dealing with accelerator facilities as it is often present in coils and magnets. Its isotopic composition was taken as 69.1% of ^{63}Cu and 30.9% of ^{65}Cu, with a density of 8.96 g/cm^3. Q values for the $^{63}\mathrm{Cu}(\gamma, n)^{62}\mathrm{Cu}$ and the $^{65}\mathrm{Cu}(\gamma, n)^{64}\mathrm{Cu}$ reactions are -10.853 MeV and -9.910 MeV respectively.

Figure 5 displays the photoneutron energy spectra simulated with the various codes. As in the case of Al in the previous section, an overall very reasonable agreement is found among all simulated spectra. They all extend up to $\sim$ 10 MeV, the maximum neutron kinetic energy one expects from

the channel ^{65}Cu$(\gamma, n)^{64}$Cu. The MCNP6 spectrum exhibits a few contributions beyond this limit which cannot come from the (γ, n) channel. Nearly no trace of individual levels is witnessed, in view of the densely packed level structure of all involved residual nuclei. The spectral shape of the Geant4 `FTFP_BERT` curve is slightly different from that obtained with other codes, somewhat favoring the 2-3 MeV energy domain at the expense of a loss of intensity for lower energies. The Geant4 `ShieldingLEND` yield is however in closer agreement to the rest of spectra in the Figure. The PHITS spectrum exhibits a step at ~ 9 MeV, coinciding with the maximum neutron kinetic energy one would expect from ^{63}Cu$(\gamma, n)^{62}$Cu (see, however, the next section concerning pre-equilibrium emission). This feature is not exhibited by other codes, as an account (effective or explicit) of the various and densely packed excitation levels of the compound/residual nucleus is included. At the high-energy end, the FLUKA and PHITS spectra are compatible, while at lower energies, the best agreement is found between PHITS and MCNP6.

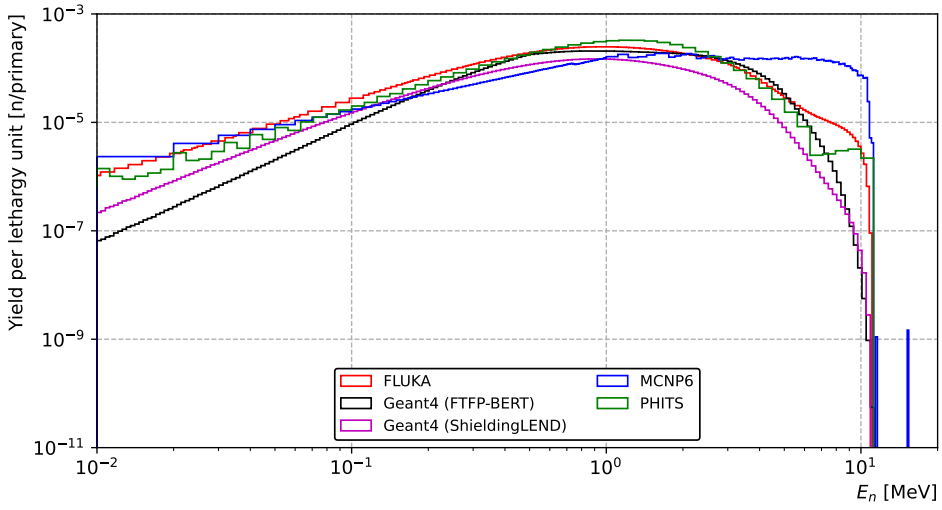

(a)

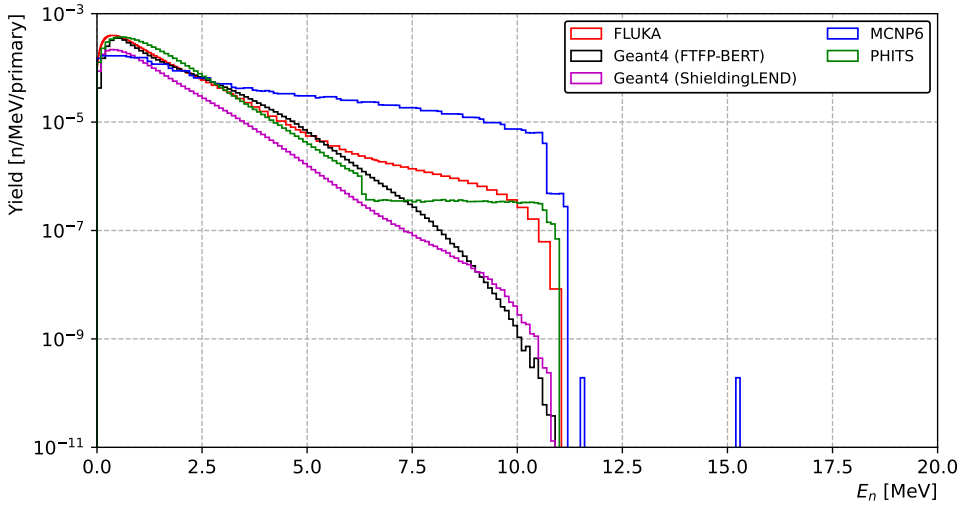

(b)

Figure 6: Simulated energy spectra of neutrons escaping the antimony target in (a) logarithmic and (b) linear energy scale.

In order to bridge the gap to the heavier target nuclei considered below (tungsten and lead), antimony has also been considered, with an isotopic composition of 57.2% ^{121}Sb and 42.8% ^{123}Sb, and a density of 6.69 g/cm^3. Q values for the $^{121}\mathrm{Sb}(\gamma, n)^{120}\mathrm{Sb}$ and the $^{123}\mathrm{Sb}(\gamma, n)^{122}\mathrm{Sb}$ reactions are -9.241 MeV and -8.960 MeV respectively.

Figure 6 displays the photoneutron energy spectra obtained from the various codes. The curves for all codes extend up to the kinematically expected limit of $\sim$ 11 MeV, the only exception being a few isolated events in the MCNP6 spectrum (seen also in the previous cases). While

FLUKA, Geant4 (both with `FTFP_BERT` and `ShieldingLEND`), and PHITS agree reasonably well on the low-energy end of the spectrum, that is, for the evaporation neutrons, differences are seen at higher energies. Concerning the FLUKA spectrum, a significant contribution from pre-equilibrium emission is obtained, becoming dominant over evaporation neutrons at energies above $\sim$ 6 MeV. The PHITS spectrum also exhibits a feature compatible with pre-equilibrium emission, although it merges a bit less smoothly onto the evaporation neutron spectral feature. The Geant4 curves instead lie a bit lower with respect to FLUKA and PHITS on the higher-energy end of the spectrum, while the MCNP6 curve is substantially higher above 5 MeV, at the detriment of the evaporation peak below 1 MeV.

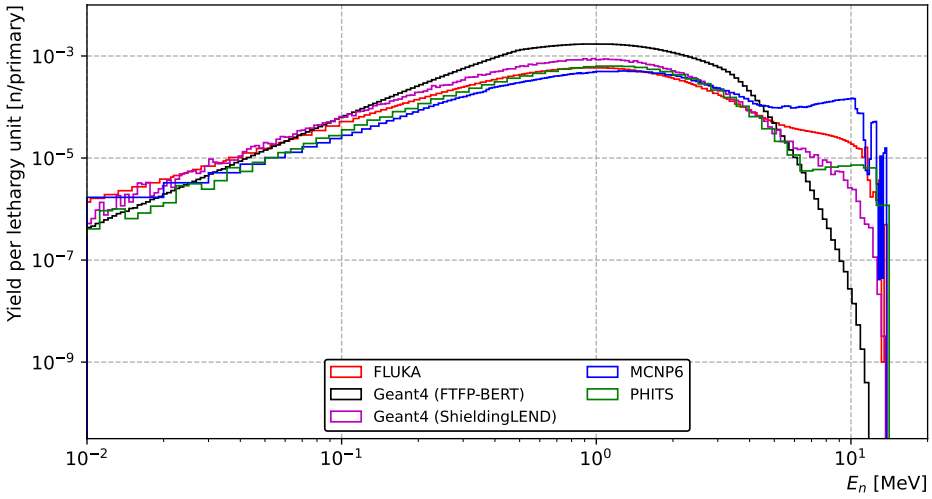

(a)

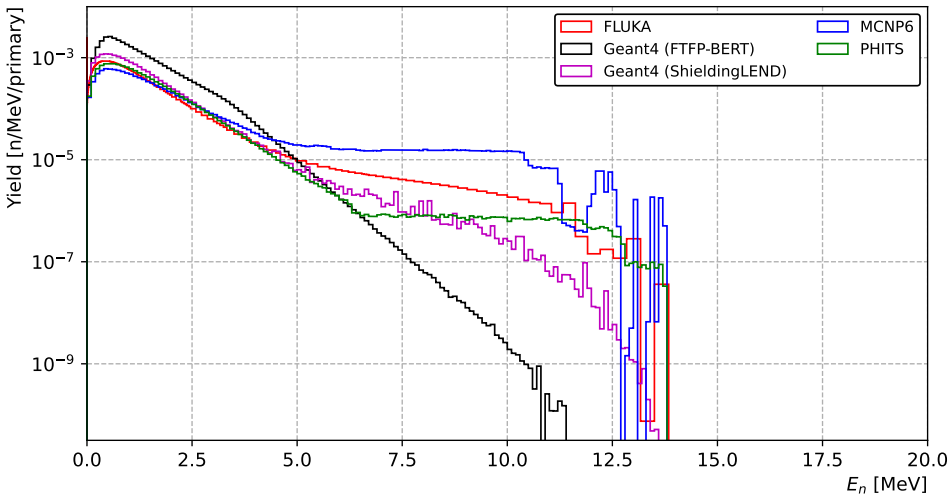

(b)

Figure 7: Simulated energy spectra of neutrons escaping the tungsten target in (a) logarithmic and (b) linear energy scale.

Next, tungsten has been considered, in view of its frequent use in particle accelerator environments for shielding and collimation. The isotopic composition was taken as ^{182}W (26.5%), ^{183}W (14.3%), ^{184}W (30.6%), ^{186}W (28.4%), with a density of 19.3 g/cm^3. The Q values for photonuclear reactions on those isotopes are respectively: -8.07 MeV, -6.19 MeV, -7.41 MeV, and -7.19 MeV. Although the levels for these high-Z isotopes are very densely packed, several peaks may still be resolved in the emitted neutron energy spectrum by virtue of having four isotopes in their natural composition. Tab. 6 displays the photoneutron energies produced by the (γ, n) channel of the four

isotopes when leaving the respective residual nuclei in the ground state. The resulting neutron energies are well separable, and are, indeed, well seen in the MCNP6 spectrum seen in Fig. 7. In the PHITS spectrum, steps are witnessed at the maximum neutron energy for the (γ, n) channel on the various isotopes, leaving the residual nucleus in the ground state, while the Geant4 curves do not exhibit them.

A significant spread among code predictions is observed for neutron energies above 5 MeV, where the yield is by and large due to pre-equilibrium emission. The latter feature is only missing in the Geant4 `FTFP_BERT` yield (it is instead captured by the Geant4 `ShieldingLEND` yield). With the 10^{10} primary histories considered here, the latter curve does not extend to the kinematically expected maximum energy of 13.75 MeV, as per Tab. 6, and suggests a higher yield of lower-energy neutrons in the 100 keV - 4 MeV domain than the rest of codes.

Isotope	Photoneutron energy [MeV]
^{182}W	11.88
^{183}W	13.75
^{184}W	12.53
^{186}W	12.76

Table 6: Expected photoneutron energy for the (γ, n) reaction channel of the isotopes of tungsten in natural composition, leaving the residual nucleus in the ground state.

3.8. Lead

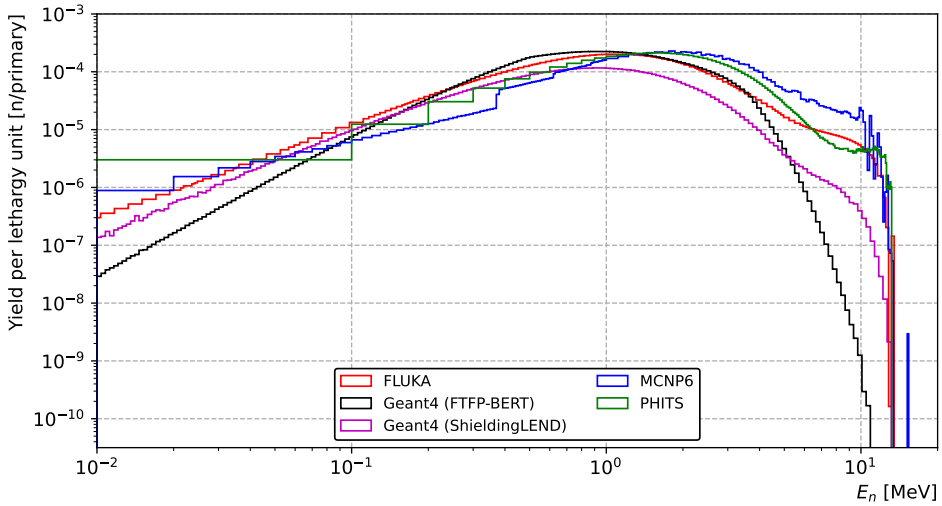

(a)

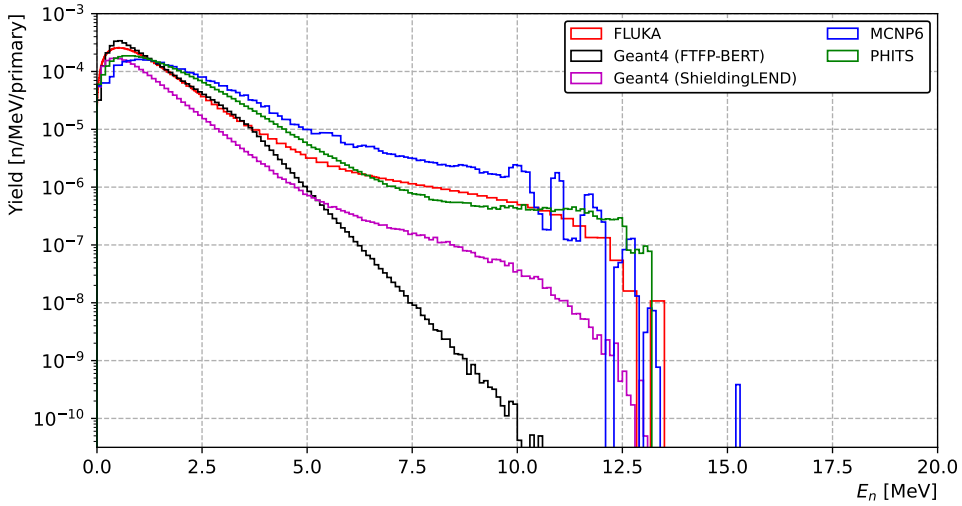

(b)

Figure 8: Simulated energy spectra of neutrons escaping the lead target in (a) logarithmic and (b) linear energy scale.

The last material considered in this benchmark is lead which, because of its high atomic number, is probably among the most used material for electromagnetic radiation shielding and is ubiquitous in nuclear facilities. Its natural isotopic composition has been considered (1.4% of ^{204}Pb, 24.1% of ^{206}Pb, 22.1% of ^{207}Pb, and 52.4% of ^{208}Pb), with a density of 11.3 g/cm^3. The Q values for photonuclear reactions on those isotopes are respectively: -8.39 MeV, -8.09 MeV, -6.74 MeV, and -7.37 MeV.

Table 7 displays the photoneutron energies expected for the (γ, n) channel on the various isotopes of lead. Photoneutron spectra simulated with the various codes are displayed in Fig. 8.

A very similar situation to that of tungsten (see the previous section) is encountered. Two main spectral features are obtained: a low-energy peak from the evaporation stage, and a higher-energy contribution from pre-equilibrium emission. Discrete peaks are still encountered in the FLUKA and MCNP6 spectra, while the PHITS spectrum appears to display steps extending to the maximum photoneutron energies expected from the (γ, n) channel on the various lead isotopes, leaving the residual nucleus in the ground state. The MCNP6 spectrum somewhat accentuates the 5-10 MeV domain compared to FLUKA and PHITS. The Geant4 `FTFP_BERT` yield underestimates the high-energy end of the spectrum, while the Geant4 `ShieldingLEND` yield is in closer agreement with the other curves, although slightly underestimating them.

Isotope	Photoneutron energy [MeV]
^{204}Pb	8.394
^{206}Pb	11.87
^{207}Pb	13.21
^{208}Pb	12.58

Table 7: Expected photoneutron energy for the (γ, n) reaction channel of the isotopes of lead in natural composition, leaving the residual nucleus in the ground state.

4. Integrated cross sections

While experimental neutron spectra differential in energy or angle are rather scarce in the literature, integrated cross sections are more abundant. Thus, whereas a comparison against experimental data at the double-differential cross-section level is not feasible, a direct comparison against integrated cross sections is generally possible. To this end, experimental integrated cross-section data available through the EXFOR [38] database have been compiled and compared with those extracted from the simulations performed in this work. In addition to the cross-section values estimated with the various MC codes considered here, as well as the experimental data, cross-sections calculated with TALYS [39] have been included in the comparison. TALYS is a deterministic code using specially developed and continuously updated reaction models to calculate particle emission probabilities for various reactions. It is used to generate the TENDL nuclear data library which is one of the most extensively used libraries by the broad nuclear physics community. For this purpose the inclusion of the results provided by this code have been considered valuable for this study. As for the MC codes, cross sections from TALYS were obtained employing the default parameter options for the various reaction models.

The results are presented in the Figure 9, which displays the cross section as a function of the mass number for the various elements considered in this study. It must be pointed out that data available from EXFOR have been measured considering the interaction of 20 MeV photons with one specific isotope of a given element. The same applies for the calculations performed using TALYS code. The calculations performed with the MC codes on the other hand considered the natural isotopic compositions. However, one can generally expect very similar cross-section values for all the isotopes of a given element, therefore, the comparison shown in the figure is accurate enough for our purpose.

The photoneutron production cross section increases with the mass of the target nucleus and reaches a plateau for heavy elements since no significant increase is observed between tungsten and lead. An exception is to be noted for light elements with a cross section for carbon lower than that of beryllium. This trend is reproduced by all the MC codes tested and by TALYS, however MCNP6, FLUKA and PHITS show better general agreement with the data than Geant4 and TALYS. In particular, TALYS displays higher cross sections for light and intermediate mass nuclei. For tungsten, all the calculated cross sections are overestimated. An interesting finding concerns PHITS, which despite showing an inaccurate simulation of the energy spectra of photoneutrons as discussed in the previous section, it is able to reproduce the same trend as the other codes for integrated cross sections. This fact strengthens the importance of the approach of this study, that is, performing benchmarks not only at the integrated cross-section level to assess production rates, but also at the differential cross-section level to better assess the energy spectrum features, for a

more comprehensive and accurate code benchmark.

Besides allowing a deeper assessment of the physics models at play in the production of photoneutrons, a comparison on the basis of the photoneutron energy spectrum, instead of just their production rate - probing the integrated cross section, is of high importance when it comes to applications involving photonuclear reactions. Indeed, the impact of neutrons, in terms of dose to organs, radiation protection of patients and workers, and materials activation inside accelerators, is strongly influenced by their energy, and not just their production rate.

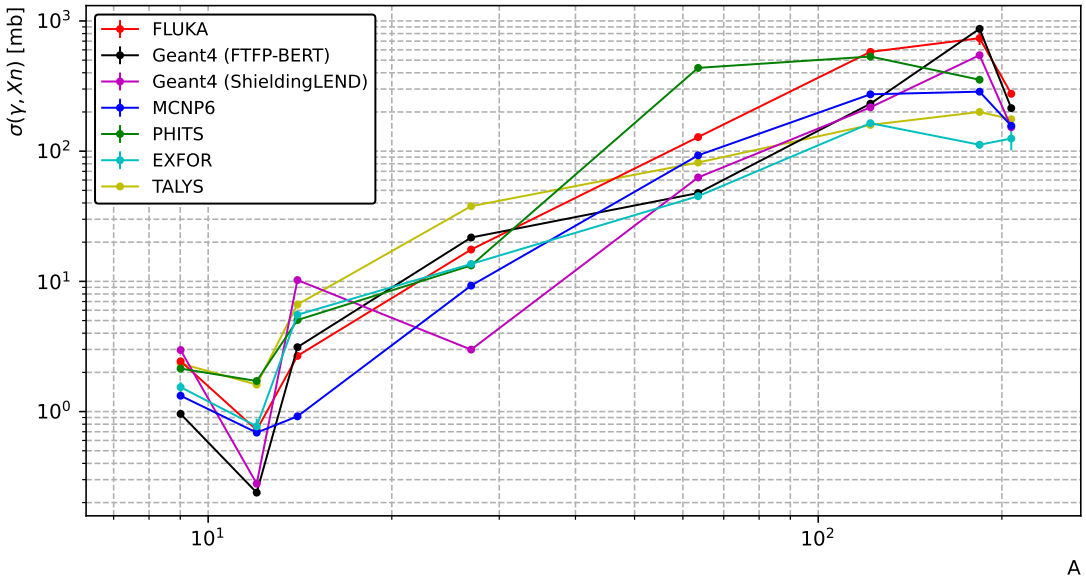

Figure 9: Integrated cross sections of the simulated materials shown as a function of the atomic mass.

5. Conclusions

As shown in this study, photoneutron spectra are heavily influenced by the nuclear level structure of the nuclei responsible for their emission, especially for light nuclei. The codes considered in this study showed significant differences in how this discretization effect is handled and in how complete the underlying level or channel information is. In particular, it was observed that PHITS, despite being a widely used and well-established code, does not account for this effect in its current distribution package when using its built-in physics models and cross-section libraries. Most recent versions of PHITS offer, however, the possibility of using other libraries which are not included in the distribution package. The latter, however, is not the default option and, therefore, was not used in this study.

The comparison of the calculated integrated neutron production cross sections with experimental data available through the EXFOR database showed that all the MC codes tested, as well as the

deterministic code TALYS, are able to reproduce the trend of increasing cross section with the mass of the target nucleus, reaching a plateau for heavy elements. However, MCNP6, FLUKA, and PHITS showed better general agreement with the data than Geant4 (with both `FTFP_BERT` and `ShieldingLEND`) and TALYS for light and intermediate mass nuclei. It is worth noting that the simulations performed with the various MC codes considered the natural isotopic compositions of the elements studied and not individual nuclei, which however are expected to yield very similar cross-section values for all isotopes of a given element.

Finally, this study highlights the importance of accurate calculations of neutron energy spectra in addition to the total production rates for applications involving photonuclear reactions and the importance of carefully checking and validating the performance of simulation codes for photonuclear reactions, especially in cases where the nuclear level structure has a significant impact on the results, typically for light target nuclei. Indeed, the dose to organs in medical applications involving high energy photons, radiation protection of patients and workers, material activation of accelerators depend strongly on the energy of the produced neutrons.

The lack of experimental data for photoneutron emission spectra is a major issue in the development and validation of MC codes for photonuclear reactions. As stated in the study, the available experimental data for comparison are provided by the EXFOR database, which offers abundant, although partial, integrated cross-section information, but a mere handful of photoneutron energy spectra. The latter do not provide sufficient information to validate the accuracy of MC simulations in reproducing the energy distribution of photoneutrons. Therefore, there is a significant need for experimental photoneutron energy, and ideally angular, distributions to further assess and improve the reliability of MC simulations in handling photonuclear reactions. Such data would enable a more extensive testing of the simulation tools available to the community. Researchers and practitioners must be aware of this limitation and take it into consideration when using MC codes for applications in which photonuclear reactions strongly contribute to the production of secondary particles.

6. Acknowledgments

This research benefited from a grant from the French National Laboratory of Metrology and Testing.

References

[1] S. Vichi, D. Dean, S. Ricci, F. Zagni, P. Berardi, D. Mostacci, Activation study of a 15mev linac via monte carlo simulations, Radiation Physics and Chemistry 172 (2020) 108758. doi:

https://doi.org/10.1016/j.radphyschem.2020.108758.
URL https://www.sciencedirect.com/science/article/pii/S0969806X19309016

[2] K. Habiger, J. Clifford, R. Miller, W. McCullough, Explosives detection with energetic photons, Nuclear Instruments and Methods in Physics Research Section B: Beam Interactions with Materials and Atoms 56-57 (1991) 834–838. doi:https://doi.org/10.1016/0168-583X(91)95041-B.
URL https://www.sciencedirect.com/science/article/pii/0168583X9195041B

[3] J. McFee, A. Faust, K. Pastor, Photoneutron spectroscopy using monoenergetic gamma rays for bulk explosives detection, Nuclear Instruments and methods in physics research A 704 (2013) 131–139.

[4] E. E. Zhuravleva, A. I. Kareva, V. B. Lopatkob, V. V. Khankinc, S. N. Cherepnyaa, V. I. Shvedunovc, Photonuclear technology for hidden explosive detection, Physics of atomic nuclei 81 (2018) 1318–1324.

[5] Besnard-Vauterin, C., Blideanu, V., Rapp, B., Development of a new method for the detection of illicit materials based on the active photon interrogation method and photo-neutron spectrometry, EPJ Web Conf. 288 (2023) 06004. doi:10.1051/epjconf/202328806004.
URL https://doi.org/10.1051/epjconf/202328806004

[6] N. Otuka, E. Dupont, V. Semkova, B. Pritychenko, A. Blokhin, M. Aikawa, S. Babykina, M. Bossant, G. Chen, S. Dunaeva, R. Forrest, T. Fukahori, N. Furutachi, S. Ganesan, Z. Ge, O. Gritzay, M. Herman, S. Hlavač, K. Katō, B. Lalremruata, Y. Lee, A. Makinaga, K. Matsumoto, M. Mikhaylyukova, G. Pikulina, V. Pronyaev, A. Saxena, O. Schwerer, S. Simakov, N. Soppera, R. Suzuki, S. Takács, X. Tao, S. Taova, F. Tárkányi, V. Varlamov, J. Wang, S. Yang, V. Zerkin, Y. Zhuang, Towards a more complete and accurate experimental nuclear reaction data library (exfor): International collaboration between nuclear reaction data centres (nrdc), Nuclear Data Sheets 120 (2014) 272–276. doi:https://doi.org/10.1016/j.nds.2014.07.065.
URL https://www.sciencedirect.com/science/article/pii/S0090375214005171

[7] V. Zerkin, B. Pritychenko, The experimental nuclear reaction data (exfor): Extended computer database and web retrieval system, Nuclear Instruments and Methods in Physics Research Section A: Accelerators, Spectrometers, Detectors and Associated Equipment 888 (2018) 31–43. doi:https://doi.org/10.1016/j.nima.2018.01.045.
URL https://www.sciencedirect.com/science/article/pii/S0168900218300627

[8] V. Blideanu, Device and method for detecting a particular substance in an object via active photonic interrogation, fR2112182 (november 2021).
URL https://patents.google.com/patent/WO2023089285A

[9] The Official CERN FLUKA website, https://fluka.cern (2022).

[10] C. Ahdida, D. Bozzato, D. Calzolari, F. Cerutti, N. Charitonidis, A. Cimmino, A. Coronetti, G. L. D'Allessandro, A. Donadon Servelle, L. S. Esposito, R. Froeschl, R. G. Alia, A. Gerbershagen, S. Gilardoni, D. Horvath, G. Hugo, A. Infantino, V. Kouskoura, A. Lechner, B. Lefebvre, G. Lerner, M. Magistris, A. Manousos, G. Moryc, F. O. Ruiz, F. Pozzi, D. Prelipcean, S. Roesler, R. Rossi, M. S. Gilarte, F. S. Pujol, P. Schoofs, V. Stransky, C. Theis, A. Tsinganis, R. Versaci, V. Vlachoudis, A. Waets, M. Widorski, New Capabilities of the FLUKA Multi-Purpose Code, Frontiers in Physics 9 (2022) 788253.

[11] G. Battistoni, T. Boehlen, F. Cerutti, P. W. Chin, L. S. Esposito, A. Fassò, A. Ferrari, A. Lechner, A. Empl, A. Mairani, A. Mereghetti, P. Garcia Ortega, J. Ranft, S. Roesler, P. R. Sala, V. Vlachoudis, G. Smirnov, Overview of the FLUKA code, Ann. Nucl. Energy 82 (2015) 10–18.

[12] A. Fasso, A. Ferrari, P. R. Sala, Designing electron accelerator shielding with FLUKA, in: Proceedings of ICRS 8, AIP, 1994, pp. 643–649.

[13] E. Fermi, High Energy Nuclear Events, Progress of Theoretical Physics 5 (4) (1950) 570–583.

[14] A. Ferrari, J. Ranft, S. Roesler, P. Sala, Cascade particles, nuclear evaporation, and residual nuclei in high energy hadron-nucleus interactions, Z. Phys. C (70) (1996) 413–426.

[15] A. Ferrari, P. Sala, The physics of high energy reactions, in: Proceedings Workshop on Nuclear Reaction Data and Nuclear Reactor Physics, Design, and Safety, World Scientific, 1998, p. 424.

[16] A. Fontana, Nuclear interaction model developments in fluka, in: Proceedings of the 14th International Conference on Nuclear Reaction Mechanisms, CERN, 2015, p. 283.
URL https://cds.cern.ch/record/2115392?ln=en

[17] A. Fasso, A. Ferrari, P. R. Sala, Photonuclear Reactions in FLUKA: Cross Sections and Interaction Models, in: CP769: International Conference on Nuclear Data for Science and Technology, AIP, 2005, pp. 1303–1306.

[18] S. Agostinelli, J. Allison, K. Amako, J. Apostolakis, H. Araujo, P. Arce, M. Asai, D. Axen, S. Banerjee, G. Barrand, F. Behner, L. Bellagamba, J. Boudreau, L. Broglia, A. Brunengo, H. Burkhardt, S. Chauvie, J. Chuma, R. Chytracek, G. Cooperman, G. Cosmo, P. Degtyarenko, A. Dell'Acqua, G. Depaola, D. Dietrich, R. Enami, A. Feliciello, C. Ferguson, H. Fesefeldt, G. Folger, F. Foppiano, A. Forti, S. Garelli, S. Giani, R. Giannitrapani, D. Gibin,

J. Gómez Cadenas, I. González, G. Gracia Abril, G. Greeniaus, W. Greiner, V. Grichine, A. Grossheim, S. Guatelli, P. Gumplinger, R. Hamatsu, K. Hashimoto, H. Hasui, A. Heikkinen, A. Howard, V. Ivanchenko, A. Johnson, F. Jones, J. Kallenbach, N. Kanaya, M. Kawabata, Y. Kawabata, M. Kawaguti, S. Kelner, P. Kent, A. Kimura, T. Kodama, R. Kokoulin, M. Kossov, H. Kurashige, E. Lamanna, T. Lampén, V. Lara, V. Lefebure, F. Lei, M. Liendl, W. Lockman, F. Longo, S. Magni, M. Maire, E. Medernach, K. Minamimoto, P. Mora de Freitas, Y. Morita, K. Murakami, M. Nagamatu, R. Nartallo, P. Nieminen, T. Nishimura, K. Ohtsubo, M. Okamura, S. O'Neale, Y. Oohata, K. Paech, J. Perl, A. Pfeiffer, M. Pia, F. Ranjard, A. Rybin, S. Sadilov, E. Di Salvo, G. Santin, T. Sasaki, N. Savvas, Y. Sawada, S. Scherer, S. Sei, V. Sirotenko, D. Smith, N. Starkov, H. Stoecker, J. Sulkimo, M. Takahata, S. Tanaka, E. Tcherniaev, E. Safai Tehrani, M. Tropeano, P. Truscott, H. Uno, L. Urban, P. Urban, M. Verderi, A. Walkden, W. Wander, H. Weber, J. Wellisch, T. Wenaus, D. Williams, D. Wright, T. Yamada, H. Yoshida, D. Zschiesche, Geant4—a simulation toolkit, Nuclear Instruments and Methods in Physics Research Section A: Accelerators, Spectrometers, Detectors and Associated Equipment 506 (3) (2003) 250–303. doi:https://doi.org/10.1016/S0168-9002(03)01368-8.

URL https://www.sciencedirect.com/science/article/pii/S0168900203013688

[19] J. Allison, K. Amako, J. Apostolakis, P. Arce, M. Asai, T. Aso, E. Bagli, A. Bagulya, S. Banerjee, G. Barrand, B. Beck, A. Bogdanov, D. Brandt, J. Brown, H. Burkhardt, P. Canal, D. Cano-Ott, S. Chauvie, K. Cho, G. Cirrone, G. Cooperman, M. Cortés-Giraldo, G. Cosmo, G. Cuttone, G. Depaola, L. Desorgher, X. Dong, A. Dotti, V. Elvira, G. Folger, Z. Francis, A. Galoyan, L. Garnier, M. Gayer, K. Genser, V. Grichine, S. Guatelli, P. Guèye, P. Gumplinger, A. Howard, I. Hřivnáčová, S. Hwang, S. Incerti, A. Ivanchenko, V. Ivanchenko, F. Jones, S. Jun, P. Kaitaniemi, N. Karakatsanis, M. Karamitros, M. Kelsey, A. Kimura, T. Koi, H. Kurashige, A. Lechner, S. Lee, F. Longo, M. Maire, D. Mancusi, A. Mantero, E. Mendoza, B. Morgan, K. Murakami, T. Nikitina, L. Pandola, P. Paprocki, J. Perl, I. Petrović, M. Pia, W. Pokorski, J. Quesada, M. Raine, M. Reis, A. Ribon, A. Ristić Fira, F. Romano, G. Russo, G. Santin, T. Sasaki, D. Sawkey, J. Shin, I. Strakovsky, A. Taborda, S. Tanaka, B. Tomé, T. Toshito, H. Tran, P. Truscott, L. Urban, V. Uzhinsky, J. Verbeke, M. Verderi, B. Wendt, H. Wenzel, D. Wright, D. Wright, T. Yamashita, J. Yarba, H. Yoshida, Recent developments in geant4, Nuclear Instruments and Methods in Physics Research Section A: Accelerators, Spectrometers, Detectors and Associated Equipment 835 (2016) 186–225. doi:https://doi.org/10.1016/j.nima.2016.06.125.

URL https://www.sciencedirect.com/science/article/pii/S0168900216306957

[20] J. Allison, K. Amako, J. Apostolakis, H. Araujo, P. Arce Dubois, M. Asai, G. Barrand,

R. Capra, S. Chauvie, R. Chytracek, G. Cirrone, G. Cooperman, G. Cosmo, G. Cuttone, G. Daquino, M. Donszelmann, M. Dressel, G. Folger, F. Foppiano, J. Generowicz, V. Grichine, S. Guatelli, P. Gumplinger, A. Heikkinen, I. Hrivnacova, A. Howard, S. Incerti, V. Ivanchenko, T. Johnson, F. Jones, T. Koi, R. Kokoulin, M. Kossov, H. Kurashige, V. Lara, S. Larsson, F. Lei, O. Link, F. Longo, M. Maire, A. Mantero, B. Mascialino, I. McLaren, P. Mendez Lorenzo, K. Minamimoto, K. Murakami, P. Nieminen, L. Pandola, S. Parlati, L. Peralta, J. Perl, A. Pfeiffer, M. Pia, A. Ribon, P. Rodrigues, G. Russo, S. Sadilov, G. Santin, T. Sasaki, D. Smith, N. Starkov, S. Tanaka, E. Tcherniaev, B. Tome, A. Trindade, P. Truscott, L. Urban, M. Verderi, A. Walkden, J. Wellisch, D. Williams, D. Wright, H. Yoshida, Geant4 developments and applications, IEEE Transactions on Nuclear Science 53 (1) (2006) 270–278. doi:10.1109/TNS.2006.869826.

[21] Geant4 Collaboration, Guide for physics lists (2023).
URL https://geant4-userdoc.web.cern.ch/UsersGuides/PhysicsListGuide/html/index.html

[22] C. J. Werner, Mcnp users manual - code version 6.2, LA-UR-17-29981.

[23] Photonuclear physics in MCNP(X), Nuclear Applications of Accelerator Technology, LA-UR-99-4827, Long Beach, California, 1999.

[24] M. Chadwick, P. Young, S. Chiba, S. Frankle, G. Hale, H. Hughes, A. Koning, R. Little, R. MacFarlane, R. Prael, , L. Waters, Cross-section evaluations to 150 mev for accelerator-driven systems and implementation in mcnpx, Nuclear Science and Engineering 131 (3) (1999) 293–328. doi:10.13182/NSE98-48.

[25] V. McLane, C. Dunford, P. Rose, Cross-section evaluations to 150 mev for accelerator-driven systems and implementation in mcnpx, BNL-NCS-44945, Brookhaven National Laboratory.

[26] M. C. White, Release of the la150u photonuclear data library, X-5:MCW-00-87(U), Los Alamos National Laboratory.

[27] T. Sato, Y. Iwamoto, S. Hashimoto, T. Ogawa, T. Furuta, S. ichiro Abe, T. Kai, P.-E. Tsai, N. Matsuda, H. Iwase, N. Shigyo, L. Sihver, K. Niita, Features of particle and heavy ion transport code system (PHITS) version 3.02, Journal of Nuclear Science and Technology 55 (6) (2018) 684–690. arXiv:https://doi.org/10.1080/00223131.2017.1419890, doi:10.1080/00223131.2017.1419890.
URL https://doi.org/10.1080/00223131.2017.1419890

[28] A. Boudard, J. Cugnon, J.-C. David, S. Leray, D. Mancusi, New potentialities of the liège intranuclear cascade model for reactions induced by nucleons and light charged particles, Phys. Rev. C 87 (2013) 014606. doi:10.1103/PhysRevC.87.014606.
URL https://link.aps.org/doi/10.1103/PhysRevC.87.014606

[29] H. Hirayama, Y. Namito, A. F. Bielajew, S. J. Wilderman, W. R. Nelson, The EGS5 code system, Tech. Rep. SLAC-R-730, KEK 2005-8 (2005).

[30] K. Iida, A. Kohama, K. Oyamatsu, Formula for proton–nucleus reaction cross section at intermediate energies and its application, Journal of the Physical Society of Japan 76 (4) (2007) 044201. arXiv:https://doi.org/10.1143/JPSJ.76.044201, doi:10.1143/JPSJ.76.044201.
URL https://doi.org/10.1143/JPSJ.76.044201

[31] S. Noda, S. Hashimoto, T. Sato, T. Fukahori, S. Chiba, K. Niita, Improvement of photonuclear reaction model below 140 mev in the phits code, Journal of Nuclear Science and Technology 52 (1) (2015) 57–62. arXiv:https://doi.org/10.1080/00223131.2014.923349, doi:10.1080/00223131.2014.923349.
URL https://doi.org/10.1080/00223131.2014.923349

[32] N. K. Sherman, R. W. Gellie, K. H. Lokan, R. G. Johnson, De-excitation neutrons following n-14 photodisintegration, Physical Review Letters 25 (1970) 114.

[33] D. Tilley, J. Kelley, J. Godwin, D. Millener, J. Purcell, C. Sheu, H. Weller, Energy levels of light nuclei a=8,9,10, Nuclear Physics A 745 (3) (2004) 155–362. doi:https://doi.org/10.1016/j.nuclphysa.2004.09.059.
URL https://www.sciencedirect.com/science/article/pii/S0375947404010267

[34] J. Kelley, E. Kwan, J. Purcell, C. Sheu, H. Weller, Energy levels of light nuclei a=11, Nuclear Physics A 880 (2012) 88–195. doi:https://doi.org/10.1016/j.nuclphysa.2012.01.010.
URL https://www.sciencedirect.com/science/article/pii/S0375947412000413

[35] J. Kelley, J. Purcell, C. Sheu, Energy levels of light nuclei a=12, Nuclear Physics A 968 (2017) 71–253. doi:https://doi.org/10.1016/j.nuclphysa.2017.07.015.
URL https://www.sciencedirect.com/science/article/pii/S0375947417303330

[36] F. Ajzenberg-Selove, Energy levels of light nuclei a = 13–15, Nuclear Physics A 523 (1) (1991) 1–196. doi:https://doi.org/10.1016/0375-9474(91)90446-D.
URL https://www.sciencedirect.com/science/article/pii/037594749190446D

[37] M. Basunia, A. Hurst, Nuclear data sheets for a = 26, Nuclear Data Sheets 134 (2016) 1–148.

[38] Experimental Nuclear Reaction Data.
URL https://www-nds.iaea.org/exfor/

[39] A. Koning, D. Rochman, Modern nuclear data evaluation with the talys code system, Nuclear Data Sheets 113 (2012) 2841.